Award No. DE-FG07-99ER15007

Project ID No. 70045
Investigation of Pore Scale Processes That Affect Soil Vapor Extraction

December 6, 2004

Lead Principal Investigator: Prof. Albert J. Valocchi
Dept. of Civil and Environmental Engineering
University of Illinois at Urbana-Champaign
205 N. Mathews
Urbana, IL 61808 (217) 333-3176 valocchi@uiuc.edu

Co-Investigators: Prof. Charles J. Werth
Dept. of Civil and Environmental Engineering
University of Illinois at Urbana-Champaign
205 N. Mathews
Urbana, IL 61808 (217) 333-3822 werth@uiuc.edu

Prof. Andrew G. Webb
Dept. of Electrical and Computer Engineering
4221 Beckman Institute
405 N. Mathews
Urbana, IL 61801 (217) 333-7480 awebb@uibrl.brl.uiuc.edu

Graduate Students Trained on the Project: 3
Julia Stammerjohn
Hongkyu Yoon
Changyong Zhang

Post-doctoral Fellows Employed on the Project: 1
Yanjie Chu

Publications Resulting from the Project:

1. Yoon, H., Valocchi, A.J., and Werth, C.W., Modeling the influence of water content on soil vapor extraction, *Vadose Zone Journal*, 2, 368-381, August 2003.
2. Chu, Y., Werth, C.W., Valocchi, A.J., Yoon, H. and Webb, A., Magnetic resonance imaging of nonaqueous phase liquid during soil vapor extraction in heterogeneous porous media. *J. Contam.,Hydrol.*, 73(1-4), 15-37, 2004.
3. Yoon, H., Valocchi, A.J., and Werth, C.W., Impact of spatially distributed nonaqueous phase liquid saturation and water content on soil vapor extraction in heterogeneous porous media, pp. 757-786, in Computational Methods in Water Resources XV, edited by C.T. Miller, M.W. Farthing, W.G. Gray, and G.F. Pinder, Elsevier, 2004.
4. Yoon, H., Valocchi, A.J., and Werth, C.W., Effect of soil moisture dynamics on dense nonaqueous phase liquid (DNAPL) spill zone architecture in heterogeneous porous media, *J. Contam.,Hydrol.*, submitted, 2004
5. Yoon, H., Valocchi, A.J., and Werth, C.W. Impact of NAPL mass transfer on mass removal mechanisms during soil vapor extraction. *In preparation.*
6. Yoon, H., Werth, C.W., and Valocchi, A.J. Impact of NAPL movement on NAPL removal mechanisms in heterogeneous porous media. *In preparation.*

7. Yoon, H., Werth, C.W., and Valocchi, A.J. Investigation of NAPL-gas mass transfer in unsaturated porous media. *In preparation.*

Executive Summary: Dense nonaqueous phase liquid (DNAPL) contamination in the vadose zone is a significant problem at Department of Energy sites. Soil vapor extraction (SVE) is commonly used to remediate DNAPLs from the vadose zone. In most cases, a period of high recovery has been followed by a sustained period of low recovery. This behavior has been attributed to multiple processes including slow interphase mass transfer, retarded vapor phase transport, and diffusion from unswept zones of low permeability. This research project used a combination of laboratory experimentation and mathematical modeling to determine how these various processes interact to limit the removal of DNAPL components in heterogeneous porous media during SVE. Our results were applied to scenarios typical of the carbon tetrachloride spill zone at the Hanford Site. Our results indicate that: (a) the initial distribution of the spilled DNAPL (i.e., the spill-zone architecture) has a major influence upon the performance of any subsequent SVE operations; (b) while the pattern of higher and lower conductivity soil zones has an important impact upon spill zone architecture, soil moisture distribution plays an even larger role when there are large quantities of co-disposed waste-water (as in the Hanford scenario); (c) depending upon soil moisture dynamics, liquid DNAPL that is trapped by surrounding water is extremely difficult to remove by SVE; (d) natural barometric pumping can remove a large amount of the initial DNAPL mass for spills occurring close to the land surface, and hence the initial spilled inventory will be over-estimated if this process is neglected.

Research Objectives: Dense nonaqueous phase liquid (DNAPL) contamination in the vadose zone is a significant problem at Department of Energy sites. Soil vapor extraction (SVE) is commonly used to remediate DNAPLs from the vadose zone. In most cases, a period of high recovery has been followed by a sustained period of low recovery. This behavior has been attributed to multiple processes including slow interphase mass transfer, retarded vapor phase transport, and diffusion from unswept zones of low permeability.

Prior attempts to uncouple and quantify these processes have relied on column experiments, where the effluent concentration was monitored under different conditions in an effort to quantify the contributions from a single process. In real porous media these processes occur simultaneously and are inter-related. Further, the contribution from each of these processes varies at the pore scale and with time.

This research aims to determine the pore-scale processes that limit the removal of DNAPL components in heterogeneous porous media during SVE. The specific objectives are to: 1) determine the effect of unswept zones on DNAPL removal during SVE, 2) determine the effect of retarded vapor phase transport on DNAPL removal during SVE, and 3) determine the effect of interphase mass transfer on DNAPL removal during SVE, all as a function of changing moisture and DNAPL content. To fulfill these objectives we used a combination of mathematical modeling and unique experimentation. In particular, we used magnetic resonance imaging (MRI) to observe and quantify the location and size of individual pores containing DNAPL, water, and vapor in flow-through columns filled with model and natural sediments. Imaging results were used in conjunction with modeling techniques to understand processes that describe the transient distribution of phases inside the column experiment. This work was then used to improve the constitutive relations in the existing multi-phase simulation model STOMP (Subsurface Transport Over Multiple Phases). The model was applied to contamination and remediation scenarios representative of the carbon tetrachloride site at Hanford. Knowledge gained form this project will allow decision makers to better assess the risk associated with vadose zone contamination and the effectiveness of SVE at hazardous waste sites.

Research Accomplishments: There were significant accomplishments in both the experimental and modeling phases of the project. These are summarized below.

A. Experimental study of desorption

Desorption column experiments were conducted to determine the effects of relative humidity on fast and slow desorption rates for different sorbate incubation periods. A silica gel and Ottawa sand were used as model sorbents. They were packed into stainless steel 0.85cm diameter columns and equilibrated at the desired relative humidity. Next, they were contaminated with vapor phase trichloroethene, incubated for different time periods, and then desorbed by purging with vapor. Desorption kinetic profiles for all columns are shown in Figures 1-4. All profiles exhibited both a fast and a slow desorbing fraction of mass. Fast desorption lasted up to 1 minute for the Ottawa sand and up to 1,000 to 10,000 minutes for the silica gel. Fast desorption was relatively instantaneous compared to slow desorption. Slow desorption was modeled using a gamma distribution of diffusion rate constants. Initial slow desorbing mass values ($M_{i,slow}$), mean diffusion rate constants (D_m/l_m^2), and gamma distribution shape factors (η) from model fits of the data are shown in Table 1. Some of the silica gel results in Table 1 are also plotted in Figure 5.

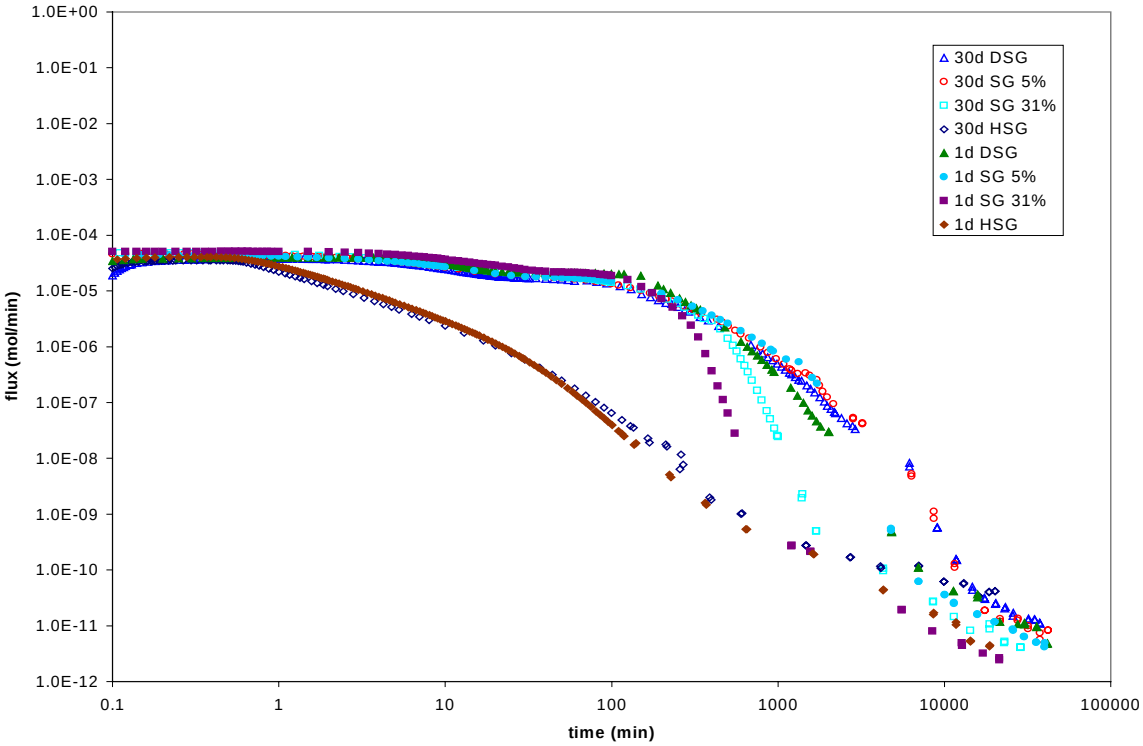

Figure 1. Silica Gel Flux Profiles

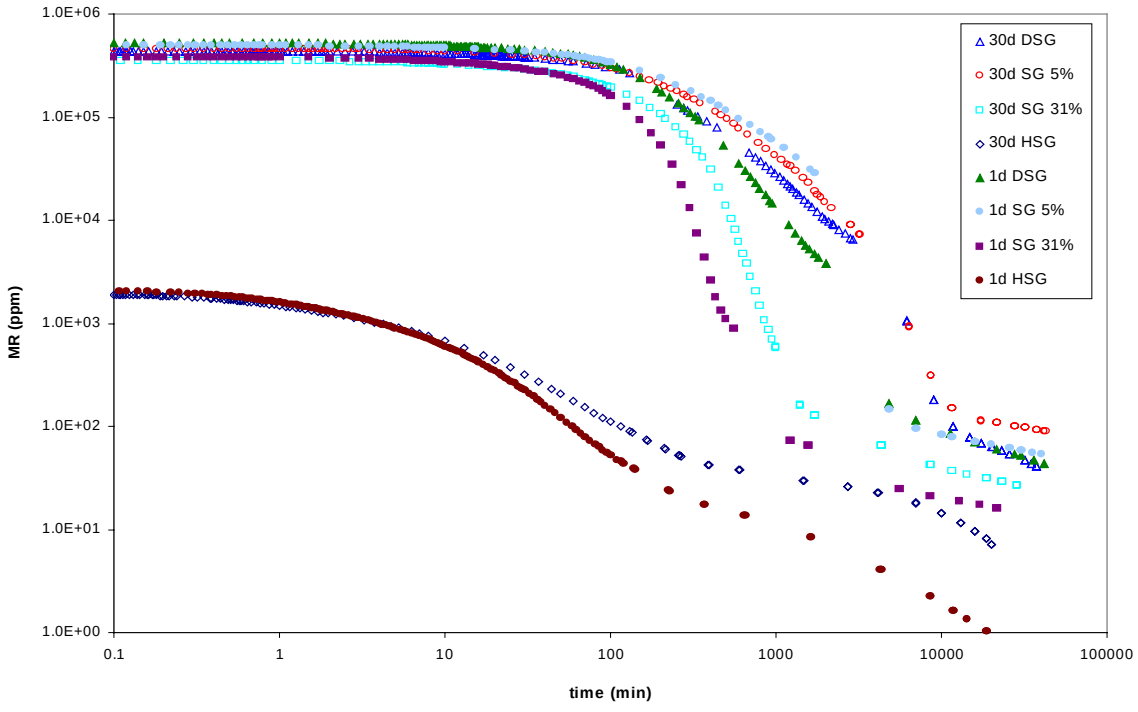

Figure 2 Silica Gel Mass Remaining Profiles

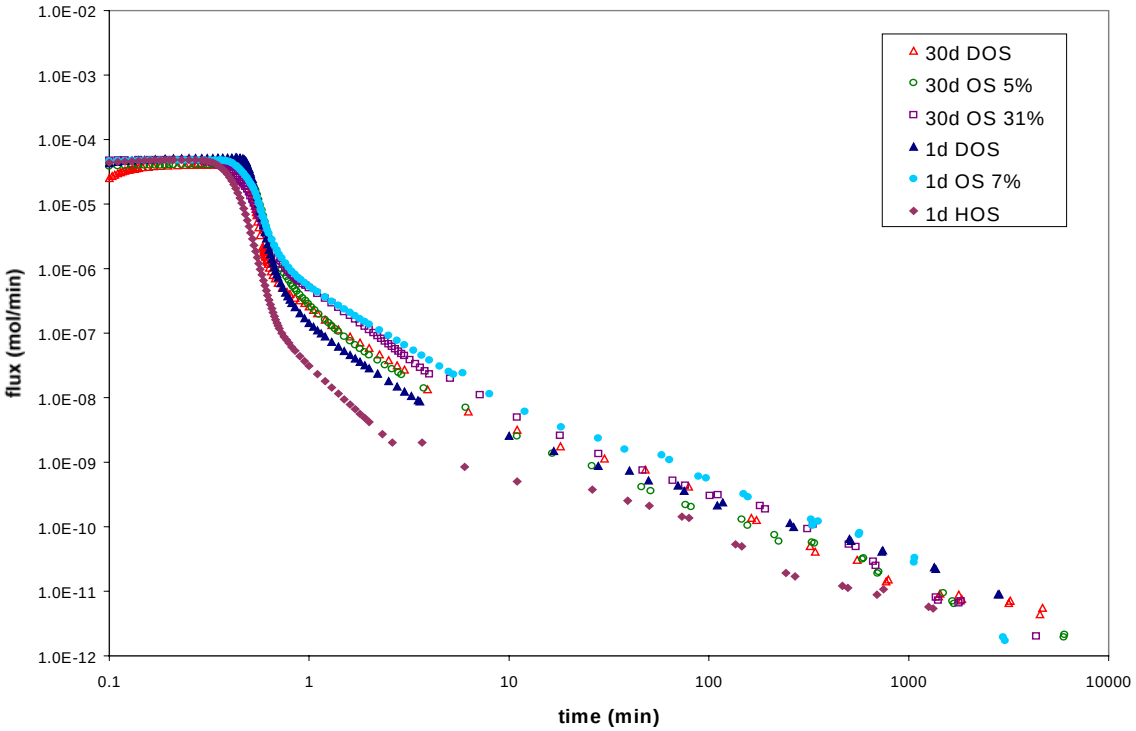

Figure 3. Ottawa Sand Flux Profiles

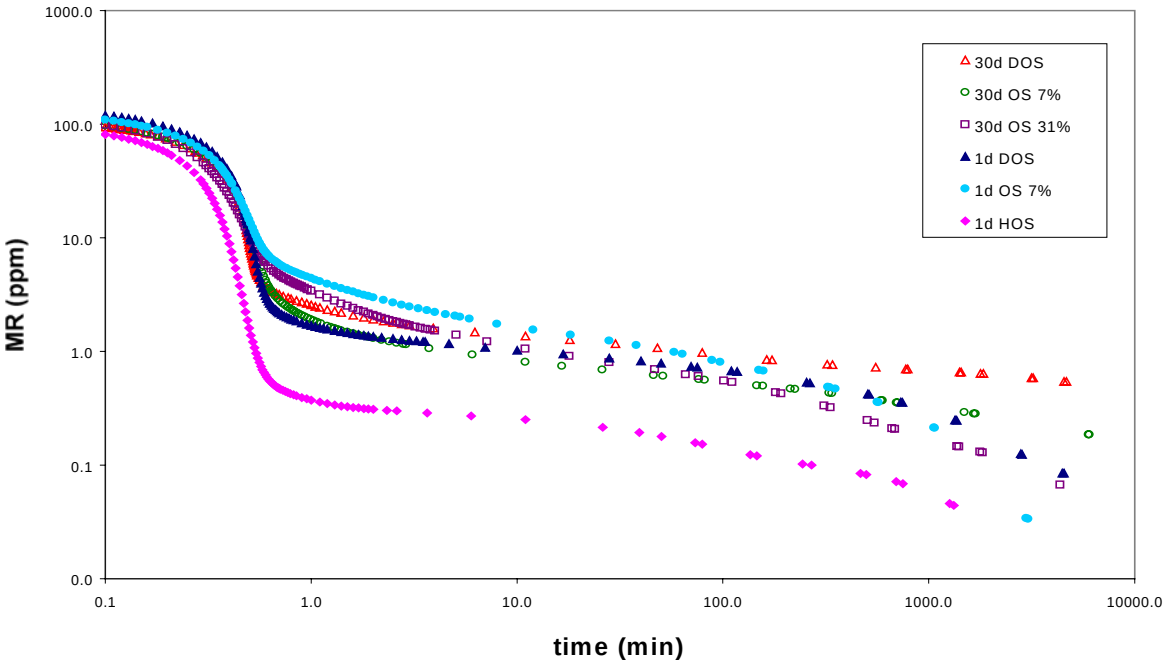

Figure 4. Ottawa Sand for Mass Remaining Profiles

Table 1. Model Characteristic Values

Sorbent	days	D_m/l_m^2	η	$M_{i,slow}$
DSG	30	1.11E-05	1.0	82.0
DSG	1	8.16E-06	1.0	94.5
5% SG	30	1.73E-05	0.283	174.5
5% SG	1	1.13E-05	0.356	96.0
31% SG	30	1.82E-05	0.443	50.7
31% SG	1	1.10E-05	0.417	24.8
HSG	30	7.38E-05	1.0	49.3
HSG	1	5.05E-04	1.0	30.1
DOS	30	9.50E-03	0.153	1.60
DOS	1	5.06E-03	0.697	1.18
7% OS	30	1.17E-02	0.249	1.14
7% OS	1	4.54E-03	1.0	2.06
31% OS	30	6.14E-03	0.428	1.65
HOS	1	5.44E-03	0.509	0.37

SG=silica gel OS=Ottawa sand
D=dry H= 100% RH

Fast desorption from the silica gel was controlled by retarded diffusion through mesopores (Werth and Reinhard, 1997). More mass was sorbed as the RH decreased. With lower RH, less water was on the silica gel surface, and more surface sites were available for TCE. This agrees with previous research that water competes with organic compounds for sorption on mineral surfaces (Chiou and Shoup, 1985; Smith et al., 1990; Ong and Lion, 1991). Because more mass sorbs at lower RH, the flux at lower RH remained higher for a longer period of time. Also, the fast flux and mass remaining dropped faster for the 100% RH column than for the 31% RH column, because less mass was sorbed in the 100% RH column. Similarly, the fast flux and mass remaining dropped faster for the 31% RH column than for the 5% RH or dry columns, because less mass was sorbed in the 31% RH column. Also the mass remaining for the 31 and 100% RH columns was affected by the time equilibrium. The flux and mass remaining values for 1 day columns at 31% and 100% RH dropped faster than the corresponding 30 day columns.

For slow desorption from silica gel, Figures 1 and 2 show that all profiles after 10,000 minutes have the same slope, indicating that desorption flux rates were similar at all RHs. Results from Table 1 support this as diffusion rate constants were similar at all RHs and equilibration times. The mass remaining during slow desorption was smaller at 100% RH than that at 31% RH, and smaller at 31% RH than at 5% RH or dry. These results suggested that as RH increases the slow mass remaining decreases. Results from Table 1 and Figure 5 support this, as initial slow desorbing mass values generally increase with decreasing RH. Also, the slow mass remaining at 31% and 100% RH was affected by the time. At 31% RH this effect was small. However, at 100% RH the profiles deviated more with time until they were more than 1 order of magnitude apart.

Previous research suggests that the slow desorption is controlled by diffusion from the micropores (Farrell and Reinhard, 1994; Werth and Reinhard, 1997) and also that water sorbs in hydrophilic micropores, but not hydrophobic micropores (Weitkamp et al., 1991). Hence, TCE may sorb to both hydrophilic and hydrophobic micropores when no water is present, but only to hydrophobic micropores when water is present. Above 31% RH it appears that water filled all of the accessible hydrophilic micropores. However, at 5% RH or in dry solids, it appears that an equal number of hydrophilic micropores were available for TCE. Since equilibration time only affected slow desorption at high RH,

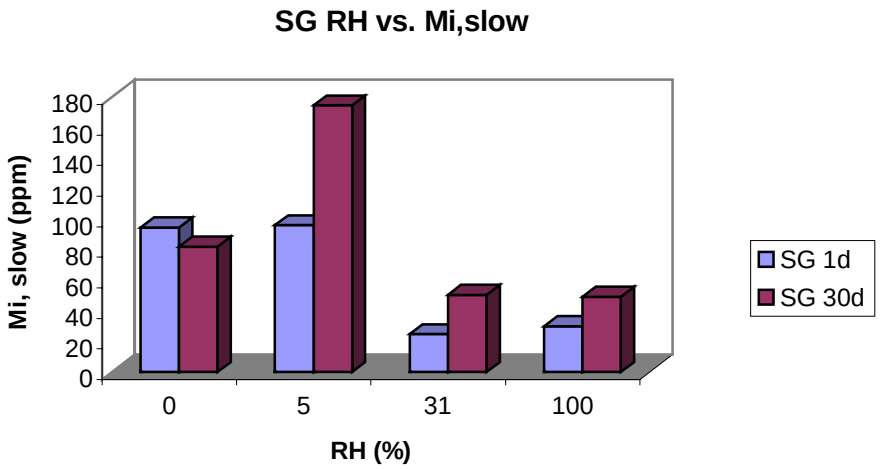

Figure 5. Model values for initial slow desorbing mass.

it also appears that water, perhaps by blocking micropore paths, increases the time required for TCE uptake. However, this result may be an experimental artifact because silica gel was exposed to a high TCE concentration for a longer time during desorption under dry conditions.

For the Ottawa sand, the fast desorbing fraction of mass dropped much faster than that for the silica gel. The Ottawa sand columns at 0% (dry), 7%, and 31% RH had similar desorption flux and MR profiles (Figures 3 and 4). The 100% RH profiles had a similar shape but decreased much faster. Hence, RH only affected fast desorption at 100% RH. Also for fast desorption, the equilibrium time did not have a clear effect on the dry or 7% RH profiles. Both 30 and 1 day desorption profiles at 31% and 100% RH were not accurately measured, so the effect of equilibration time could not be determined at these RHs.

For slow desorption, flux and mass remaining profiles for the dry, 7%, and 31% RH columns were the same. The slow desorption flux for the 100% RH column started lower than at other RHs, but this difference decreased until 40 minutes. For the rest of the desorption time, the desorption flux profiles had the same slope, indicating that desorption rates at all conditions were similar. Results in Table 5 support this, as diffusion rate constant values were similar. In contrast, mass remaining values at 100% RH were below all others. Again results in Table 5 support this as the initial slow desorbing mass was smaller at 100% RH than at other RHs.

As with silica gel, it appears that water was driven out of Ottawa sand micropores during baking, allowing more mass to sorb at RHs below 100%. Why different mass remaining values were not observed at 31% RH and 7% RH is not clear. Perhaps some hydrophilic micropores only fill above 31% RH.

B. Magnetic Resonance Imaging Experiments on SVE

A unique feature of our project was the development and use of magnetic resonance imaging (MRI) experimental techniques to directly observe the amount and location of NAPL in flow-through columns during simulated SVE. MRI is unique because it is non-destructive, allowing three-dimensional images to be taken of the phases as a function of space and time. Our results are described in detail in Chu et al. (2004); to our knowledge, our work is the first time MRI has been used to observe both water and NAPL in unsaturated media.

Analysis of the MRI data focused on four column experiments. These columns were packed with silica gel grains in three ways: coarse grains (250-550 μm) only, fine grains (32-63 μm) only, and a core of fine grains surrounded by a shell of coarse grains. All columns were initially saturated with water and then drained under a constant suction head. After drainage, the columns were contaminated with decane, and then drained to different decane saturations. The column with only coarse grains and one of the core-and-shell columns was drained to residual decane saturation. The column with only fine grains and the remaining core-and-shell column were drained such that the fine grains were initially above residual. After decane drainage, each column was then continuously purged with water saturated nitrogen gas and magnetic resonance imaging (MRI) was used to observe and quantify the amount and location of NAPL in the columns over time.

Analysis of the MRI data for all four columns yielded three main results. First, at residual saturation, a sharp volatilization front moved through the columns filled with either coarse or fine-grain silica gel only. A numerical model developed by Yoon et al. (2003) was applied to these columns, and mass transfer coefficients for decane volatilization were obtained by fitting NAPL saturation profiles. Mass transfer rate constants for both columns were greater than literature values. In previous work, mass transfer coefficients were obtained by fitting models similar to ours to vapor phase concentrations of NAPL in the column effluent. Small variations in column temperature and pressure give rise to significant errors in measured effluent concentrations. Hence, we hypothesized that previously determined mass transfer coefficients are in error, and use of the NAPL saturation profile will provide more accurate mass transfer coefficient for NAPL volatilization.
Second, in the heterogeneous column at residual saturation, the volatilization front in the core lagged just behind that in the shell. This is illustrated below in Figure 6. Pressure drops across all columns were measured; these were used to calculate flow rates in the core and shell of the heterogeneous columns. With these, advection and diffusion rates of decane vapor from the fine grain core were compared to advection rates of decane vapor from the coarse grain shell. This analysis indicated that advection dominated mass removal from the coarse-grain shell. But in the fine-grain core, mass removal was controlled diffusion radially outward from the core to the clean part of the shell.

Third and last, when decane in the core of the heterogeneous column was above residual saturation, decane volatilization occurred near the inlet, the relative decane saturation throughout the core dropped uniformly, and decane in the core flowed in the liquid phase to the shell to replenish volatilized decane. This is illustrated below in Figure 7. Hofstee et al. (1997) measured capillary-pressure saturation curves for a nonspreading NAPL (tetrachloroethene) in a three-phase (air-water-NAPL) system. Above residual saturation, applied suction was required to displace the NAPL with air, indicating that capillary forces held the NAPL in place above residual saturation, and that gradients in capillary pressure could potentially cause flow. Also Hayden and Voice (1993) observed by cryo-scanning electron microscopy with X-ray analysis that in a three-phase (air-water-NAPL) porous media system, a non-spreading NAPL forms continuous films and lenses at intermediate saturations. This indicates that when decane was above residual saturation in our system, it was continuous and capillary pressure gradients during purging caused it to flow.

A more detailed discussion of the imaging results presented here is in our publication (Chu et al., 2004). It is important to note that our results are directly applicable to the Hanford site, where SVE is actively being used to remediate carbon tetrachloride. Like decane, carbon tetrachloride is a nonspreading chemical. Hence, we suspect that in fine grain sediments, carbon tetrachloride removal is limited by diffusion when it is at or below residual saturation, and possibly by capillary-driven flow to higher permeability regions where volatilization is occurring when it is above residual saturation.

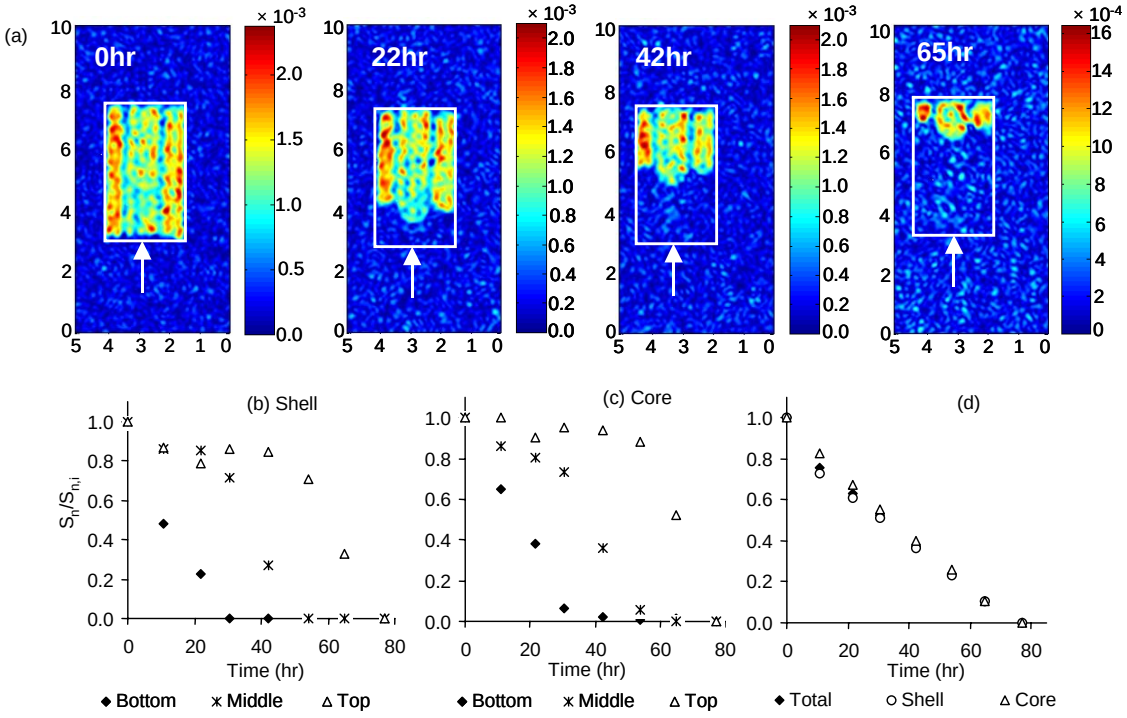

Figure 6. Column 3: Core (fine) and shell (coarse) column initially at residual decane saturation: (a) Image slices were obtained at different times. Only the center image of 22 slices is shown at each time point. Horizontal and vertical scales are in centimeters. The menu bar intensity is proportional to the decane saturation. (b) Change of the relative decane saturation (S_n/S_{ni}) with time in bottom, middle and top sections of the shell. (c) Change of the relative decane saturation (S_n/S_{ni}) with time in bottom, middle and top sections of the core. (d) Change of the relative decane saturation (S_n/S_{ni}) with time in the whole column.

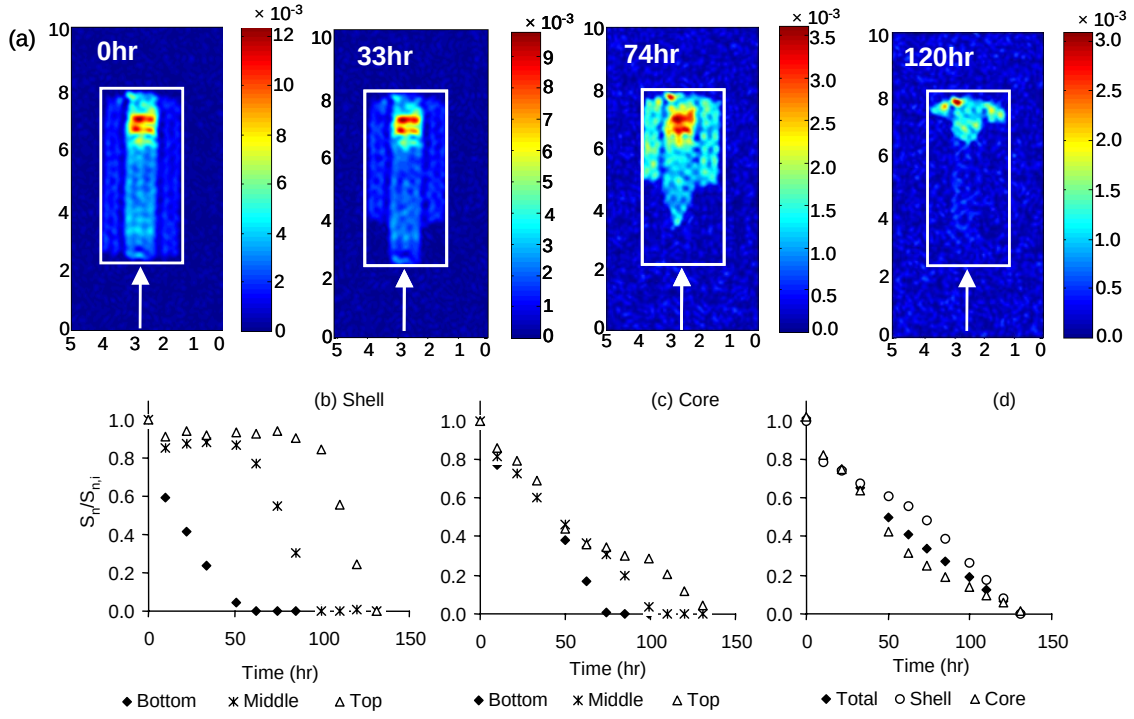

Figure 7. Column 4: Core (fine) and shell (coarse) column with core initially above residual decane saturation: (a) Image slices obtained at different times. (a) Image slices were obtained at different times. Only the center image of 22 slices is shown at each time point. Horizontal and vertical scales are in centimeters. The menu bar intensity is proportional to the decane saturation. (b) Change of the relative decane saturation (S_n/S_{ni}) with time in bottom, middle and top sections of the shell. (c) Change of the relative decane saturation (S_n/S_{ni}) with time in bottom, middle and top sections of the core. (d) Change of the relative decane saturation (S_n/S_{ni}) with time in the whole column.

C. Mathematical Modeling to Study Impact of Temperature and Moisture Content on SVE

In arid environments it is possible that the relatively dry air that enters the soil during SVE may cause evaporation to occur, resulting in a change in soil temperature and a decrease of water saturation. In order to study these processes a set of one-dimensional models were developed and analyzed. Details are published in Yoon, et al. (2003). The model incorporates the following processes: (a) advection and dispersion of vapor-phase contaminants; (b) equilibrium or mass-transfer controlled desorption from the aquifer solids; (c) equilibrium partitioning into the water phase; (d) mass-transfer limited volatilization and dissolution of the separate NAPL phase. The contaminant transfer and transport model was coupled with moisture flow and heat transport to investigate the effect of water saturation and temperature changes on NAPL mass transfer, vapor phase retardation, and slow desorption during SVE. A relationship developed in the literature was used to express the fraction of soil surface area exposed to the vapor phase as a function of water saturation. Also, a new constitutive relationship between the NAPL-gas mass transfer rate and the water saturation was developed based on data in the literature.

The coupled model was used to investigate the effect of water saturation and temperature changes on SVE cleanup time. Simulations over a 5m distance were performed for two scenarios: low water saturation in a high permeability soil (Case I) where the gas flow rate is high, soil drying is expected and vapor sorption to soil may be important, and high water saturation in a low permeability soil (Case II) where the gas flow

rate is low and NAPL mass transfer to the gas phase is rate-limited. Input parameters for Case I were based on the Hanford sandy soil and input parameters for Case II were based on the Hanford silty sand and Plio-Pleistocene (Caliche) soil. Gas flow rates were chosen in the range from 10 to 100 m/d at low water saturation and 0.5 m/d at high water saturation. These gas flow rates are similar to those encountered at the Hanford SVE site and many other sites beyond the vicinity of an extraction well. Simulation parameters varied in Case I and II are shown in Table 2.

Run 1 is defined by intermediate values of all input parameters obtained from the literature. For CASE I the time to remove NAPL, 95% of the sorbed mass, and 99% of the sorbed mass was calculated in Figure 8, while for CASE II only the time to remove NAPL was calculated as shown in Figure 9 since the time scale required for the mass removal was similar for the NAPL and sorbed phases. Two sets of simulations for cases of low and high water saturation revealed the following: (see Yoon et al., 2003, for further details)

(1) At low water saturation (CASE I) in high permeability soils, the time to removal the sorbed mass was markedly prolonged by slow desorption (Runs 1 and 9). NAPL mass was removed very fast relative to other processes due to high NAPL-gas mass transfer rates and high gas flow rates. Even at low RH (25 %) and high gas flow rate, soil drying was slow relative to NAPL removal (Runs 1 and 4) and the effects of water evaporation on NAPL removal were marginal. Also, water evaporation (Runs 1and 2), the fraction of slow desorbing mass (Runs 1 and 11), and Freundlich parameters (Runs 1 and 13-15) affected the cleanup time, however, the effect was marginal.

(2) At high water saturation (CASE II) in low permeability soils, the efficiency of mass removal was primarily controlled by NAPL removal. The prolonged cleanup time was most significant in runs having a low dissolution rate (Runs 1 and 3) and β (Runs 1 and 4-5) in which a higher β value represents a high water saturation. For these cases, NAPL mass transfer was limited by diffusion through the water phase. Simulation results indicated that the limiting NAPL removal mechanism changed from volatilzation to dissolution (i.e., diffusion through surrounding water) as soil moisture increased. This was accounted for in the parameter β. The effect of the total simulation length scale was examined in Runs 6 and 7. For Runs 2 and 7 with a high k_{dis} (1.5×10^{-6} s^{-1}) the cleanup time was nearly proportional to the length, while for Runs 1 and 6 with a lower k_{dis} (1.5×10^{-7} s^{-1}) the cleanup time differed by only 25 %. These results imply that in many heterogeneous field situations, the cleanup time will be significantly influenced by diffusion through the water phase even over a short length of contaminant zones at high water saturation.

(3) For all cases simulated, temperature and water content changes due to water evaporation were only marginally important in our one-dimensional system. Results in this study indicate that simplified models that neglect temperature change and water evaporation are valid under most field conditions.

Table 2. Parameters varied in simulations

CASE I: Parameters varied in low water saturation simulations

RUN	Evapo-ration	q (m/d)	Relative Humidity (%)	k_{ws} (s^{-1})	$k_{gn,i}$ (s^{-1})	f_{vmt}	f_{veq}‡	K_{F2}(mg/kg)/ (mg/l)^{n}F2
RUN 1	ON	50	50	8.E-07	0.01 §	0.4	0.0218(20%)	100
RUN 2	OFF							
RUN 3				8.E-07 †				
RUN 4			25					
RUN 5		10			0.003 §			
RUN 6		100			0.015 §			
RUN 7				4.E-06				
RUN 8				4.E-07				
RUN 9				1.E-07				
RUN 10					1.E-05			
RUN 11						0.6		
RUN 12								500
RUN 13							0.11 (4.56%)	500
RUN 14							0.05 (10.0%)	725
RUN 15			25				0.25 (1.76%)	500

CASE II: Parameters varied in high water saturation simulations

RUN	k_{dis} (s^{-1})	β	Length (m)
RUN 1	1.5E-07	4.4	5
RUN 2	1.5E-06		
RUN 3	1.5E-05		
RUN 4		3.0	
RUN 5		0‡	
RUN 6			2
RUN 7	1.5E-06		2

Run 1 is a reference case for CASE I and CASE II. Other Runs use the parameters in Run 1 except where values are given

CASE I:

† k_{ws} is not a function of temperature for this run.

‡ The value in parentheses is the initial water saturation corresponding to f_{veq}.

§ $k_{gn,i}$ is from the empirical correlation presented by Wilkins et al. (1995).

CASE II:

$k_{gn,i}$ (0.00004) is from the empirical correlation presented by Yoon et al. (2002).

‡ k_{gn} is constant (=$k_{gn,i}$)

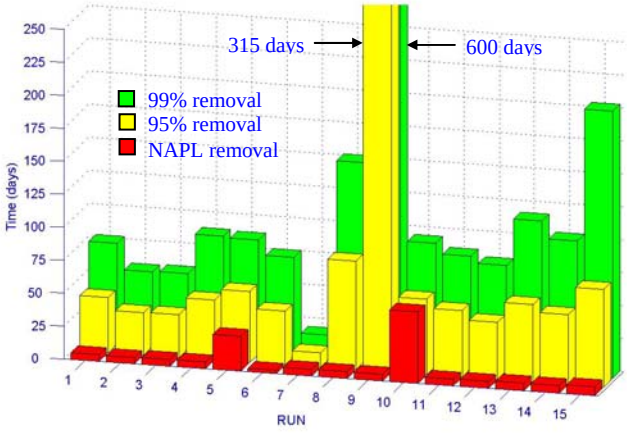

Figure 8. Cleanup time for CASE I in Table X.

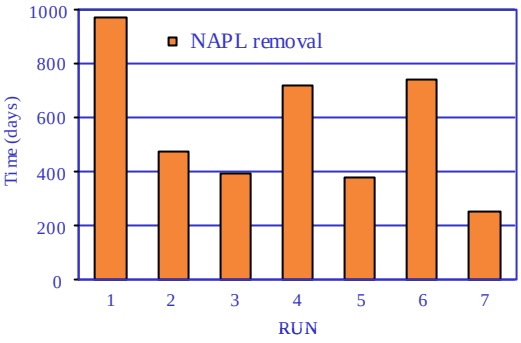

Figure 9. Cleanup time for CASE II in Table X.

D. Field-Scale Mathematical Modeling Using STOMP

The final phase of our project focused on a computational investigation of the effect of soil-moisture dynamics on the DNAPL spill-zone architecture, and the contaminant transport and removal mechanisms during soil vapor extraction in heterogeneous porous media. Our preliminary results were presented at the International Conference on Computational Methods in Water Resources (Yoon et al., 2004a), and we have just submitted a manuscript (Yoon et al., 2004b) reporting details of our findings regarding the effect of soil-moisture dynamics on the DNAPL spill-zone architecture in heterogeneous systems. To accomplish these tasks, a multiphase flow simulator, STOMP (Subsurface Transport Over Multiple Phases), was used to develop a new conceptual model for the migration and distribution of a DNAPL spill affected by simultaneous disposal of wastewater. In addition, we modified the exiting STOMP simulator. The modifications were based upon knowledge gained in the MRI experiments and our earlier detailed one-dimensional modeling reported in Yoon et al. (2003). The modified STOMP code now includes slow desorption and mass transfer from trapped NAPL, which were dominant rate-limited mass transfer processes during SVE (Yoon et al., 2003).

This final phase of the research is investigating the core hypothesis that the spatial distribution of NAPL saturation, water content, and soil permeability determines the pore-scale processes that control SVE and the time scales for cleanup. It is now understood that there are three forms of NAPL phase in the vadose zone: free NAPL that is mobile and in contact with gas, residual NAPL that is immobile and in contact with gas, and trapped NAPL that is immobile and surrounded by water (Lenhard et al., 2004). We used a new permeability-saturation-pressure (k-S-P) constitutive model that considers all three NAPL forms. Diffusion of trapped NAPL through surrounding pore water to the gas phase is likely to be slow. Hence, we believe that the spatial distribution of total, trapped, and residual NAPL saturation must be accounted for, as well as the corresponding permeability fields, to determine rate-limiting mass transfer processes during SVE.

Numerical simulations for a two-dimensional stratified system based on the Hanford site near the CCl_4 discharge area (e.g., the 216-Z-9 Trench) were performed. STOMP was first used to distribute NAPL in heterogeneous porous media, and then to simulate NAPL removal during SVE. The numerical domain and boundary conditions are presented in Figure 10. Hydraulic properties of the porous media used in this study are listed in Table 3. The grid was refined in both PPlc and PPlz layers and near the NAPL release boundary. The sequential indicator simulation model (SISIM) from the GSLIB package (Deutsch and Journel, 1998) was used to generate a two-dimensional random permeability field consisting of three discrete soil types for the heterogeneous layers. The random fields were generated by conditioning upon data that were arbitrarily selected, based upon Hanford data (Khaleel and Freeman, 1995; Rohay, 2000; Serne et al., 2002; William et al., 2002). Each layer is statistically independent with anisotropy ratios (kx/kz) of 5 and 10 for the heterogeneous and homogeneous layers, respectively. The water table was placed 6 m from the bottom boundary and was inclined at 0.005 from left to right.

Table 4 summarizes the simulations that were performed for six different cases to illustrate the effects of heterogeneity, barometric pumping, water recharge rates, and water saturation on the distribution and migration of NAPL. Case 1 is considered the base case; it is the most representative of the Hanford CCl4 site based upon the literature, and the permeability field is the one shown in Figure 10. Water and NAPL recharge rates for Case 1 are divided into two stages. During Stage I, wastewater and NAPL recharge occurred over a 7 year period (between 1955 and 1962) in the Trench. The NAPL recharge was modeled in batch mode; the recharge rate was increased to four times higher than the annual NAPL recharge rate in FigureD-2 for 0.025 years, followed by a zero NAPL recharge rate for 0.075 years. This cycle was repeated for 7 years.

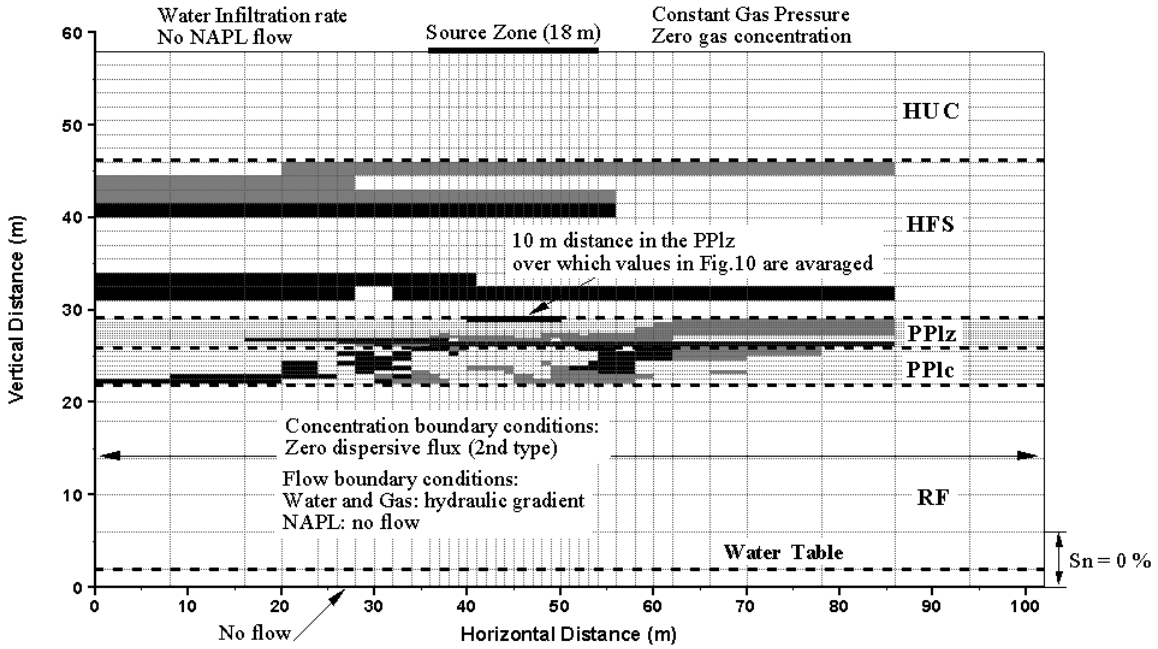

Figure 10. Numerical domain, boundary conditions, and distribution of heterogeneous permeability in stratigraphic units (Case 1). White stands for mean permeability and black and gray colors stand for permeability an order of magnitude lower and higher than a mean value in each layer, respectively.

Table 3. Porous media properties used in simulations [a]

Stratigraphic Units [b]		k [(1)] (m^2)	Depth (m)	Variance	Range (m) [c]	Global (%) [d]	ϕ [(1)]	λ [(2)]	ψ_d [(3)] (cm)	S_{lr} [(4)]	$S_{nt,max}$ [(5)]	K_d [(6)] (L/kg)
HUC	Mean	6.8E-11	12	-	-	100	0.166	1.0	8.8	0.12	0.10	0.5
	Low	6.6E-13				20	0.382	0.503	25.4	0.20	0.25	
HFS	Mean	6.6E-12	15.5	0.12	45, 1.5	60	0.382	0.503	15.4	0.15	0.20	0.5
	High	6.6E-11				20	0.382	0.503	10.4	0.10	0.15	
	Low	1.7E-14				15	0.424	0.303	70.0	0.40	0.25	
PPlz	Mean	1.7E-13	3	0.12	15, 1.2	70	0.52	0.303	60.0	0.25	0.25	1.0
	High	1.7E-12				15	0.424	0.303	40.0	0.20	0.18	
	Low	7.8E-13				20	0.337	0.720	60.4	0.25	0.25	
PPlc	Mean	7.8E-12	4	0.5	9, 0.9	60	0.337	0.720	40.4	0.25	0.20	0.5
	High	7.8E-11				20	0.337	0.720	20.4	0.25	0.15	
RG	Mean	1.3E-11	22	-	-	100	0.226	0.538	50.4	0.10	0.10	0.1

[a] Maximum residual NAPL saturation was set at 0.05.
[b] Indicator classes are based on the three soil classes and no nugget effect. Low and high values represent permeability an order of magnitude lower and higher than a mean value in heterogeneous layer, respectively.
[c] Horizontal and vertical ranges
[d] Soil composition for each layer
(1) Permeability, Khaleel and Freeman (1995) and Oostrom et al. (2003).
(2) Brooks and Corey pore geometry index, Khaleel and Freeman (1995) and Yoon et al. (2003)
(3) Air entry pressure, Khaleel and Freeman (1995) and Yoon et al. (2003)
(4) Residual water saturation, Khaleel and Freeman (1995)
(5) Maximum trapped NAPL saturation, Essaid et al. (1993), Oostrom et al. (2004), and White et al. (2004)
(6) Linear sorption coefficient, Yonge et al. (1996) and Truex et al. (2001)

Table 4. Conditions used in simulation cases [a]

Case	Permeability Field [b]	Barometric Pumping	Artificial Water recharge	Natural Water Infiltration (m/yr)	Initial Condition
1	Heterogeneous	No	Yes	0.005-0.075[c]	Dry
2	Heterogeneous				
3	Uniform				
4		Yes			
5			No	0.30[d]	
6			No	0.30[d]	Wet

[a] Case 1 is the reference case. Other Cases use conditions defined in Case 1 except where conditions are described.
[b] Anisotropy ratios of 5 and 10 were used for heterogeneous and uniform fields, respectively.
[c] A rate of 0.005 m/yr from March to October and a rate of 0.075 m/yr from November to February were repeated. This cycle was repeated for the entire simulation period.
[d] A water infiltration rate of 0.30 m/yr for 0.025 years was followed by no water infiltration for 0.075year. This cycle was repeated for the entire simulation period.

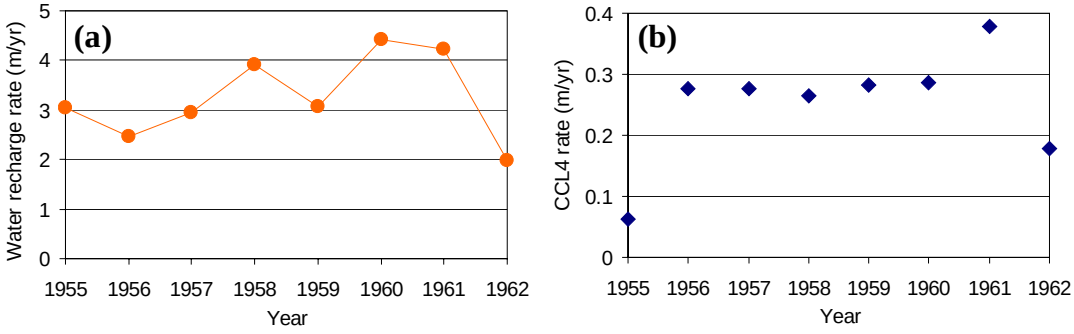

Figure 11. Estimated water (a) and CCl_4 (b) recharge rates through the trench on the top boundary at the Hanford site.

The wastewater recharge was modeled as a continuous source (Piepho, 1996). Total discharged NAPL and wastewater volumes in this case were the same as those in Figure 11. Natural water recharge rates were maintained over the entire top boundary during Stage I, and during Stage II, which lasted an additional 31 years. No further NAPL or wastewater recharge occurred during Stage II.

Cases 2 and 3 are used to investigate the effects of heterogeneity on NAPL migration and distribution in the vadose zone. For Case 2, different permeability field realizations for the PPlc and PPlz layers were chosen, while all other layers were the same as in Case 1. In particular, the PPlz layer in Case 2 has a discontinuity in subunits of a low permeability soil type underneath the source zone. For Case 3, a uniform field for each layer with an anisotropy ratio of 10 was used (Piepho, 1996; Oostrom et al., 2003b). The logarithmic mean permeability for each layer was very similar to the average values in Cases 1 and 2.

Case 4 is used to investigate the effects of barometric pressure fluctuations on NAPL migration and distribution. At the Hanford Site, barometric pressure fluctuations averaged about 1.3% of the average value (Rohay, 1996), but no simulations reported in the literature have taken this into account. These fluctua-

tions were approximated with a square wave in which the cycle of high and low pressures within ± 0.65 % of the average pressure was repeated every 0.02 years. This pressure fluctuation was accounted by changing the top boundary condition. All other conditions are the same as those in Case 1.

Cases 5 and 6 are used to investigate the effects of water recharge rate on NAPL migration and distribution in the vadose zone with different initial water saturations. For these cases, artificial water recharge to the Trench was not considered, and a water infiltration rate of 0.30 m/yr for 0.025 years was followed by no water infiltration for 0.075 years. This cycle was repeated for the entire simulation period. The DNAPL recharge scenario was the same as in Case 1. For Case 5 (dry case), the initial water distribution was the same as in Case 1. For Case 6 (wet case), the initial water distribution was obtained by conducting a long-term simulation using a sequence of water infiltration rates: 0.15 m/yr for 0.025 years followed by no water infiltration for 0.075 years.

The distributions of total NAPL saturation, trapped NAPL saturation, and residual NAPL saturation after 38 years for Case 1 are shown in Figure 12. CCl_4 mass in the vadose zone, CCl_4 mass across the water table, and volatilized CCl_4 mass out of the domain after 38 years were presented in Figure 13. Simulation results for each case were compared with those of the base case, Case 1. Summarizing, NAPL mass distribution was affected slightly by the permeability fields (Cases 1, 2, and 3), significantly by the barometric pumping (Cases 1 and 4), significantly by water infiltration rate for initially dry conditions (Cases 1 and 5), and moderately by the initial water distribution (Cases 1 and 6). Simulations for six cases revealed the following (see Yoon et al., 2004b, for further details):

(1) Comparison of the distribution and transport of CCl_4 for three different permeability fields (Cases 1-3) demonstrates that the overall permeability and connectivity of low permeability soil in the PPlz and PPlc layers were important factors controlling the NAPL distribution. Although the NAPL distributions after 38 years were not the same for Cases 1 through 3, dominant processes affecting NAPL migration for Cases 2 and 3 were the same as for Case 1 as shown in Figure 14. For instance, NAPL migrated downward quickly due to the high water and NAPL recharge rates, and the formation of trapped NAPL in the low permeable layers was not important. Since residual NAPL is immobile, it slowed NAPL migration and left CCl_4 mass behind, of which most in the upper region volatilized. This leads us to conclude that the effect of different patterns of heterogeneous permeability on the NAPL distribution was overwhelmed by high water and NAPL recharge rates during Stage I.

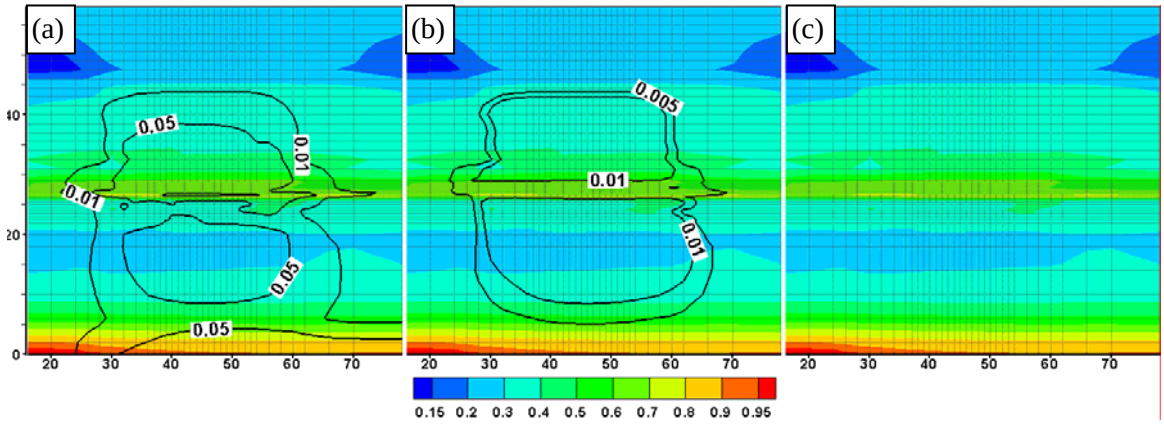

Figure 12. Snapshots of (a) total NAPL saturation, (b) trapped NAPL saturation, and (c) residual NAPL saturation (Case 1) at 38 years. Color bar stands for water saturation and contour lines stand for NAPL saturation.

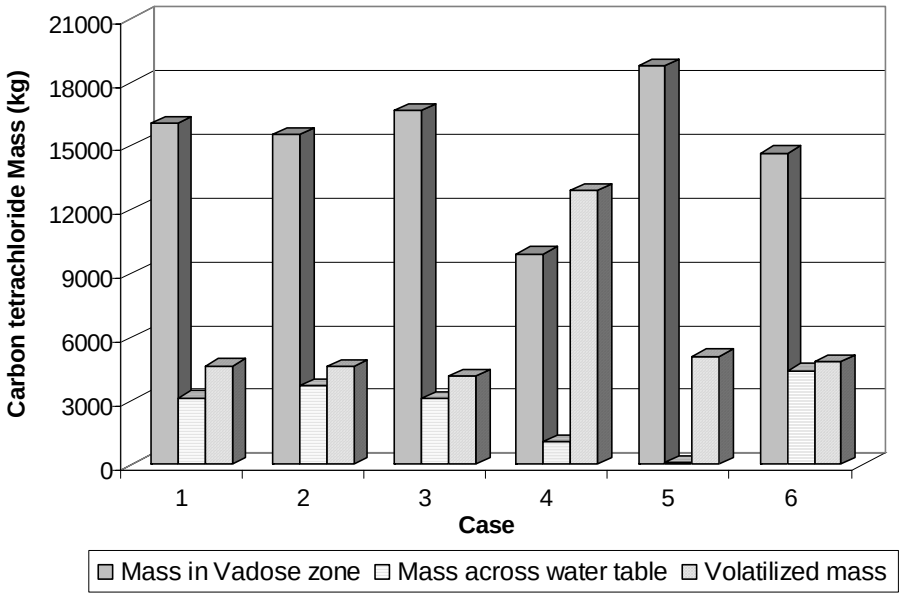

Figure 13. Comparison of CCl_4 mass in the vadose zone, CCl_4 mass across water table, volatilized CCl_4 mass out of the domain after 38 years.

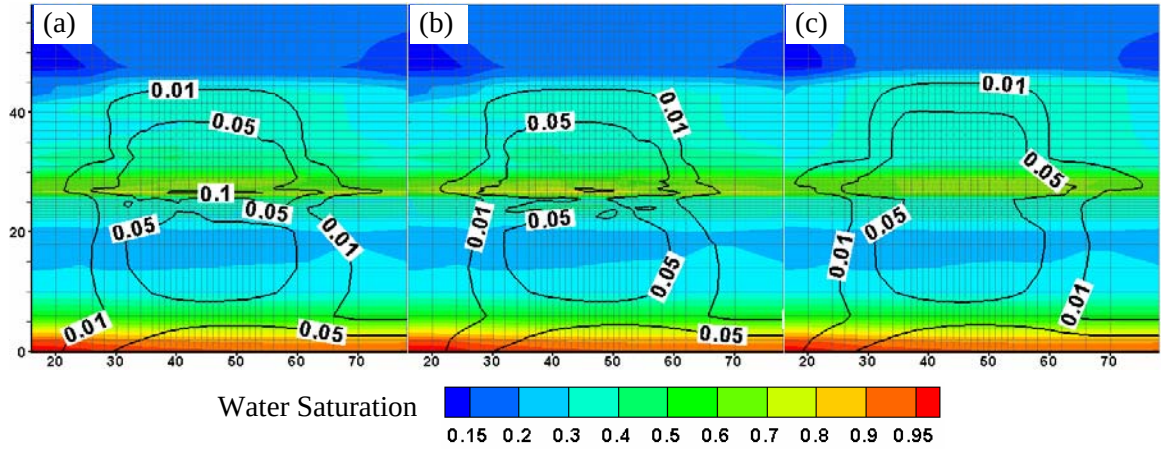

Figure 14. Comparison of total NAPL saturation after 38 years: (a) Case 1, (b) Case 2, and (c) Case 3. Contours indicate NAPL saturation and color bar indicates water saturation.

(2) Comparison of results with and without barometric pumping (Cases 1 and 4) showed that barometric pumping had a dramatic impact upon NAPL migration (Case 4) during Stage I when the NAPL phase existed at the source zone, resulting in high advective mass flux into the atmosphere (Figure 13). During Stage I, the flux of CCl_4 vapor into the atmosphere through the top boundary was approximately an order of magnitude greater with barometric pumping than without barometric pumping (Figure 15). Gas concentrations at the source zone were at the saturation vapor pressure during NAPL discharge. Barometric pumping induces gas phase advection, which caused this high concentration gas to leave the model domain when the pressure at the ground was less than the pressure in the subsurface. Vertical pressure gradients induced by barometric pressure fluctuations caused CCl_4 vapor to move up and down and offset the horizontal pressure gradients induced by the dense vapor above the low permeability layers. Hence, compared to Case 1, the gas concentration was low near the left- and right- boundaries (Figure 16 (a) and (b)). During Stage I, high water saturation in a low permeability sub-layer in the HFS enhanced the horizontal advective gas flow in Case 4. Although gas concentrations at the boundary in Case 4 were much lower than those in Case 1 (Figure 16), CCl_4 vapor mass out of the domain through the side boundaries above the PPlz layer in Case 4 was greater than that in Case 1 due to a high horizontal gas flow related to the barometric pumping (Figure 15).

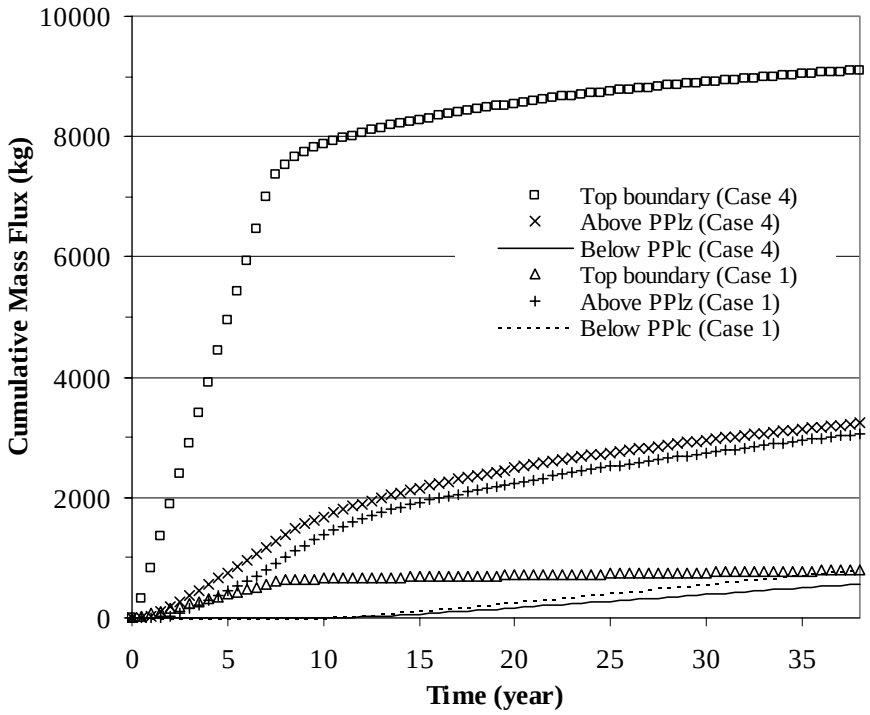

Figure 15. Comparison of cumulative volatilized mass fluxes out of the domain (Cases 1 and 4)

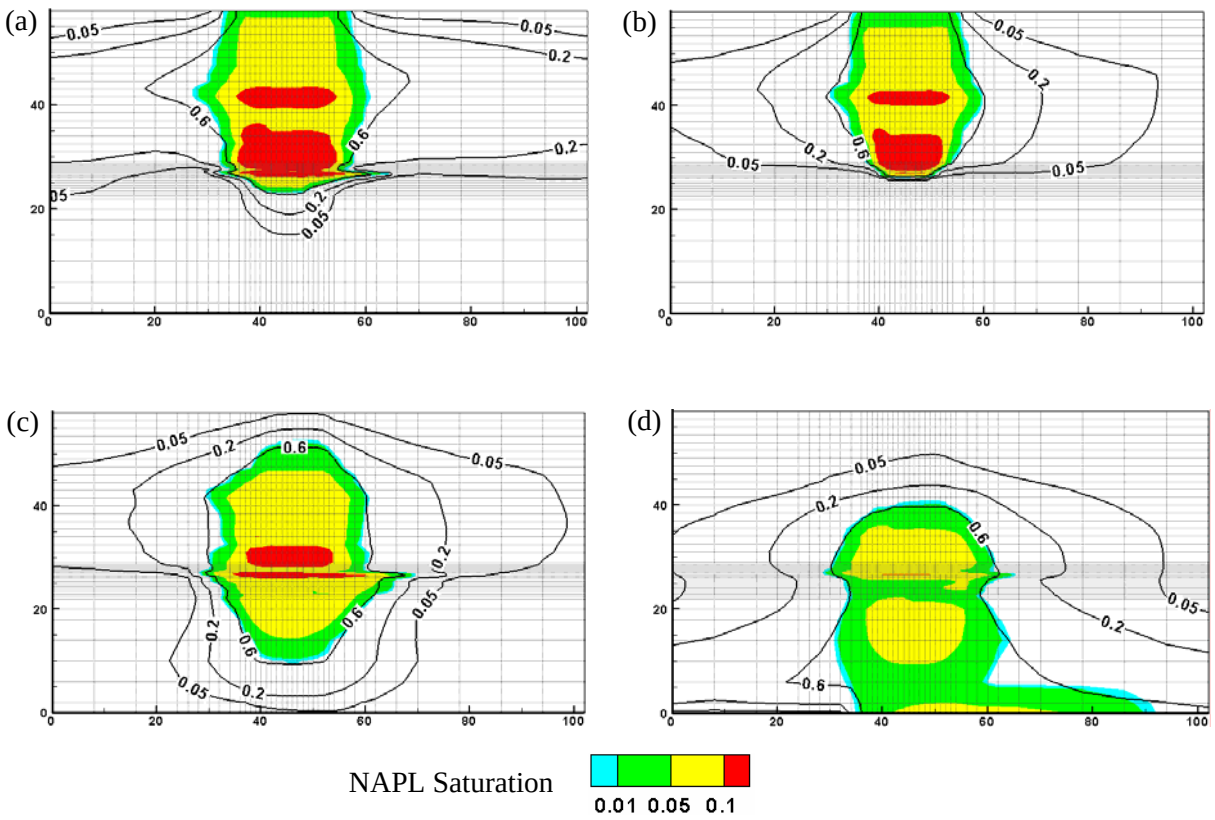

Figure 16. Snapshots of total NAPL saturation (color bar) and gas concentrations (g/L, contour lines) at (a) 5 yr (Case 1), (b) 5 yr (Case 4), (c) 8 yr (Case 4), and (d) 38 yr (Case 4).

(3) Comparison of results between Cases 1 and 5 (Figure 17) showed that NAPL flow was significantly affected by the high water discharge rates that resulted in high water saturation and high NAPL relative permeability during Stage I in Case 1. These results indicate that proper water infiltration rates must be considered in order to predict NAPL migration and distribution in the vadose zone. In contrast to Cases 1 and 6, results for Case 5 showed that water saturation had a great influence upon the trapped NAPL saturation. In contrast to what would be expected in semi-arid regions like the Hanford Site, the formation of trapped NAPL in a water-wetting system was limited by a high water recharge rate that caused the vadose zone to be very wet before the NAPL front reached the low permeability layers. This high water saturation resulted in a continuous wetting phase providing infiltrating water with high water relative permeability during Stage I. Hence, the formation of trapped NAPL is not likely to be a dominant process at the Hanford site, despite high water and DNAPL discharge rates. Instead, NAPL likely exists in the residual and free form.

(4) It should be noted that for all cases, volatilization was responsible for removing NAPL saturation in the upper region of the domain where residual NAPL is a high portion of total NAPL. This implies that at the field scale, volatile organic contaminants are likely to volatilize into the gas phase, resulting in smaller residual NAPL saturation than observed in the laboratory. These results indicate that in the field, residual NAPL saturation is strongly dependent on the change in water saturation and volatility. Since most laboratory experiments on the formation of residual NAPL were performed in a closed system for a short time

period, further study on the formation of residual NAPL in an open system over a long time period is needed. In addition, due to the dependence of the form of NAPL upon soil moisture dynamics, prediction of NAPL distribution in the vadose zone requires initial water distribution and infiltration data in heterogeneous porous media.

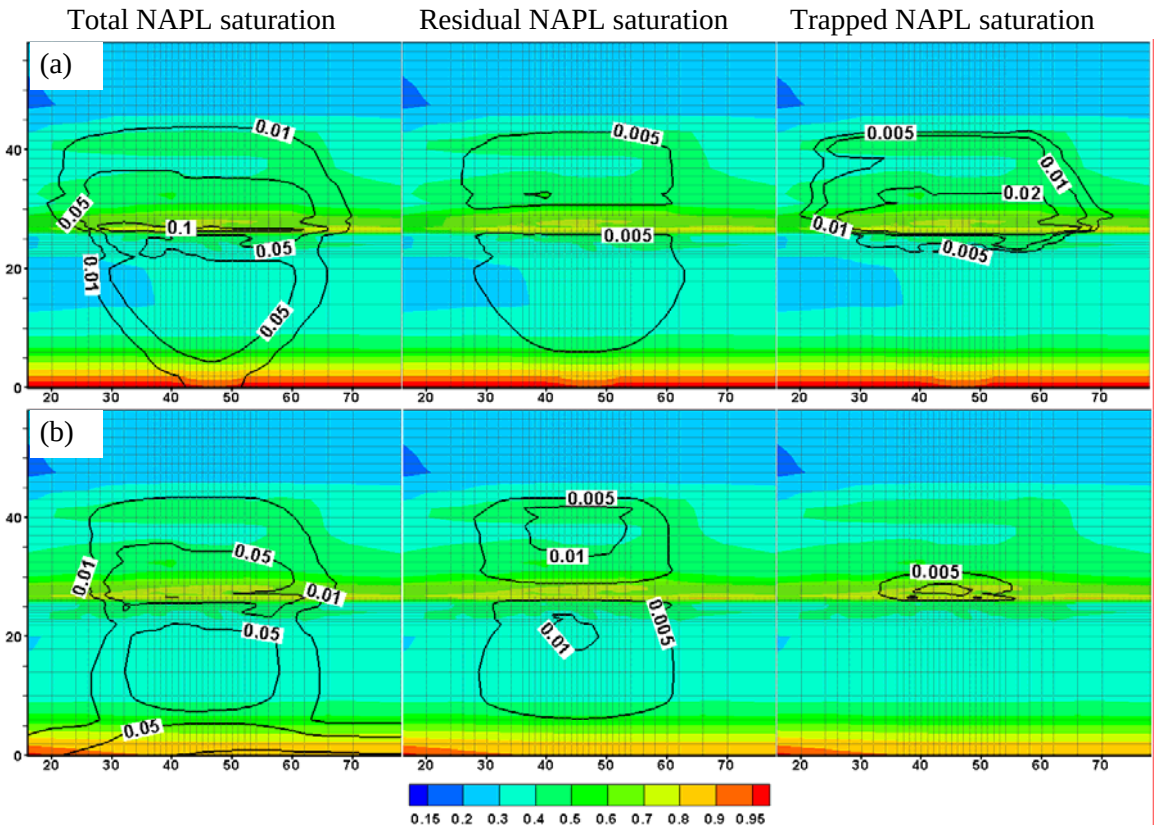

Figure 17. The distributions of total NAPL saturation, residual NAPL saturation, and trapped NAPL saturation after 38 years: (a) Case 5 and (b) Case 6. Color bar stands for water saturation and contour lines stand for NAPL saturation.

Although site-specific conclusions cannot be drawn quantitatively, this study gives important insights into the nature, extent, and mass of the DNAPL in a thick heterogeneous vadose zone similar to conditions at the Hanford Site. The extent of lateral spreading and the mass across the water table might be reduced significantly by mass lost to the atmosphere due to barometric pumping. The presence of the PPlz layer slowed the vertical migration of DNAPL. The effect of local heterogeneity, however, was offset by soil moisture dynamics considered in this study. The extent of contaminant vapor flux to the atmosphere at the ground surface will depend upon the distance between the ground surface and the NAPL source zone; fluctuations of temperature and pressure at the ground surface will affect these rates as well. These results lead us to conclude that taking into account barometric pumping is essential to develop a conceptual model for the distribution and migration of NAPL, especially for NAPL spill events at the ground surface. This study also indicates that consideration of the formation of residual NAPL and dynamic boundary conditions in the context of full three-phase flow (e.g., fluctuation of precipitation) are needed. In addition, these results imply that in many heterogeneous field situations, the cleanup time will be significantly

influenced by diffusion through the water phase from the trapped NAPL at high water saturation in low permeability zones during SVE.

Soil vapor extraction wells are placed in the same depths at different locations based on Hanford SVE extraction systems. Simulation of SVE was performed for 7 years by specifying gas flow rates through extraction wells. The NAPL distributions at 38 years in Cases 1 and 5 served as initial conditions for SVE. Since SVE is applied to remove contaminants in the unsaturated zone, contaminants located below the water table surface were not considered during SVE. Equilibrium partitioning among NAPL, gas, and aqueous phases was assumed for Case I where trapped NAPL was negligible. Simulations of equilibrium partitioning among phases and slow mass transfer rate (10^{-7} s^{-1}) from trapped NAPL for Case 5 were performed. Slow desorption was not considered. The water infiltration rate during SVE is 0.5 cm/yr. The results of SVE simulations indicate the following:

(1) As expected, most of NAPL was removed from high permeability layers and diffusion from a low permeability layer is a dominant process for low removal rate at later time during SVE as shown in Figures 5 and 6. For all simulated cases total NAPL saturations after 7 years of SVE (Figures 18 and 19) are very similar. It is important to note that trapped NAPL in the Hanford fine sand layer for the non-equilibrium case became free or residual NAPL due to a decrease of water saturation and then was removed by fast volatilization. The change of various NAPL forms and water saturation during SVE should be considered.

(2) Trapped NAPL may persist even after long term SVE operation due to slow dissolution rate.
For the equilibrium partitioning case, trapped NAPL that exists at the NAPL plume boundary dissolves very fast and volatilizes. Then, volatilized NAPL in the low permeability layer diffuses toward the advective gas flow in the high permeability zone, as shown in Figure 20(a). Hence, the NAPL plume shrinks as trapped NAPL at the boundary is removed. For the non-equilibrium case, trapped NAPL is dissolved slowly and mass removal occurs by volatilization of free NAPL inside the NAPL plume which then diffuses toward the advective gas flow, as shown in Figure 20(b). Hence, the NAPL plume does not shrink, but rather trapped NAPL is left along the boundary. In the presence of trapped NAPL, the rate-limited mass transfer from trapped NAPL in low permeability zones should be considered during SVE.

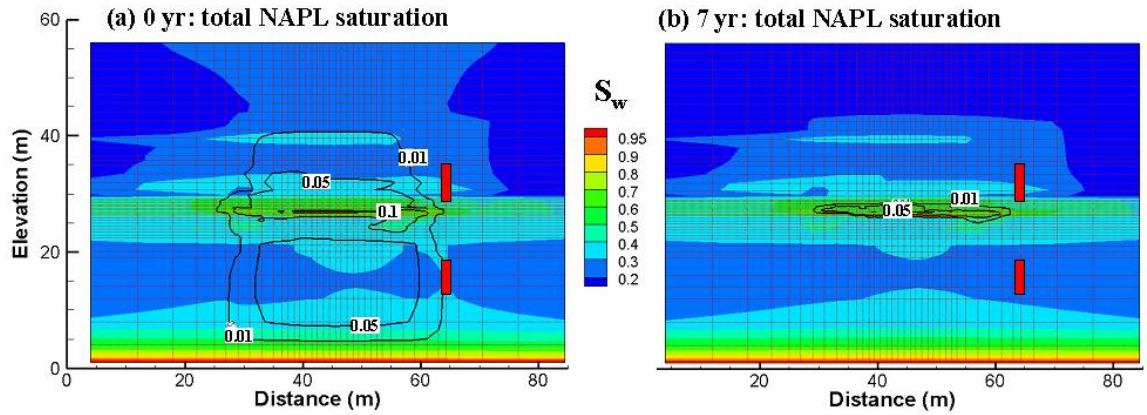

Figure 18. Total NAPL saturation at (a) 0 years and (b) 7 years for Case 1. Color bar stands for water saturation and contour label stands for NAPL saturation. Vertical columns are extraction wells at same locations.

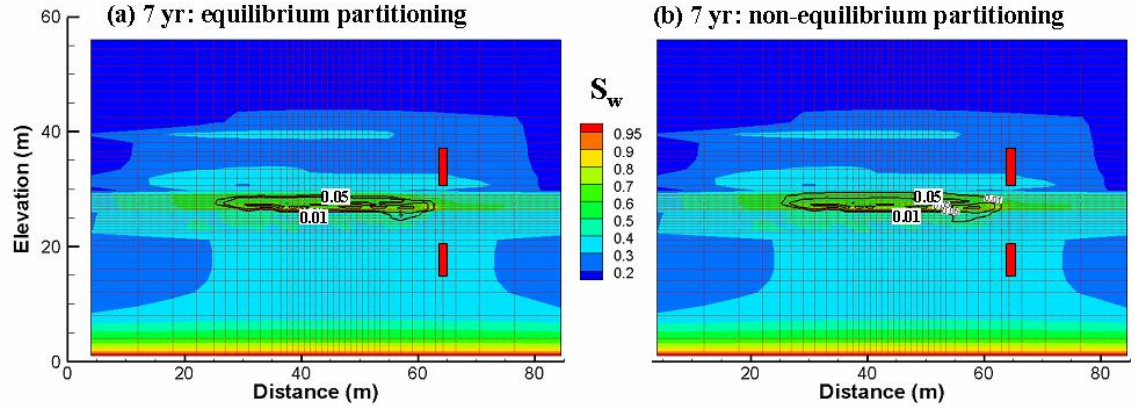

Figure 19. Total NAPL saturation at 7 years for (a) equilibrium partitioning and (b) non-equilibrium partitioning for Case 5. Color bar stands for water saturation and contour label stands for total NAPL saturation. Vertical columns are extraction wells at same locations.

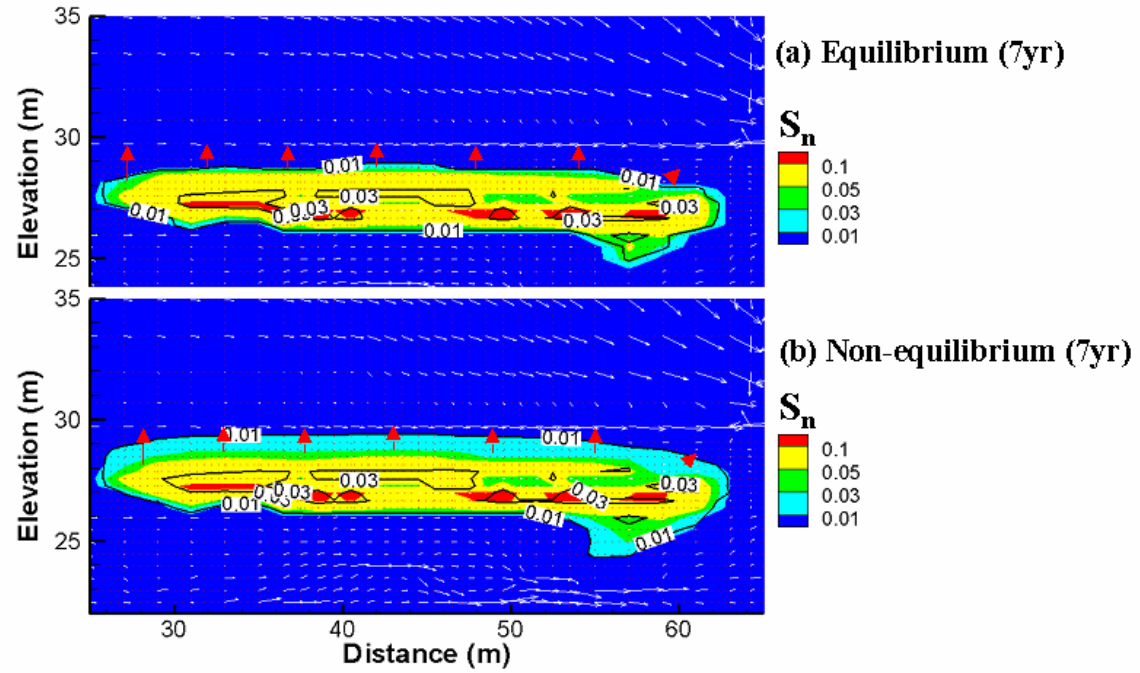

Figure 20. NAPL saturation at 7 years for (a) equilibrium partitioning and (b) non-equilibrium partitioning for Case 5. Color bar stands for total NAPL saturation and contour label stands for trapped NAPL saturation. Arrows on the NAPL plume indicate a diffusion process. Gas flow rate field is shown. The magnitude of arrow is proportional to gas flow rate.

List of References:

Chiou, C.T., and T.D. Shoup. 1985. Soil sorption or organic vapors and effects of humidity on sorptive mechanism and capacity. Environ. Sci. Technol. 19:1196-1200.

Chu, Y., Werth, C.W., Valocchi, A.J., Yoon, H. and Webb, A., Magnetic resonance imaging of nonaqueous phase liquid during soil vapor extraction in heterogeneous porous media. *J. Contam.,Hydrol.*, 73(1-4), 15-37, 2004.

Deutsch, C.V., Journel, A.G., 1998. GSLIB Geostatistical Software Library and User's Guide. Oxford University Press, NY.

Farrell, J. and M. Reinhard. 1994. Desorption of halogenated organics from model solids, sediments, and soil under unsaturated conditions: 1. Kinetics. Environ. Sci. Technol. 28:63-72.

Hayden, N.J., and T.C. Voice. 1993. Microscopic observation of NAPL in a three-fluid-phase soil system. J. Contam. Hydrol. 12: 217-226.

Hofstee, C., Dane, J.H., Hill, W.E., 1997. Three-fluid retention in porous media involving water, PCE, and air. J. Contam. Hydrol. 25, 235-247.

Khaleel, R., and E.J. Freeman. 1995. Variability and scaling of hydraulic properties for 200 area soils, Hanford Site. Report WHC-EP-0883. Westinghouse Hanford Company, Richland, WA.

Lenhard, R.J., Oostrom, M., Dane, J.H., 2004. A constitutive model for air-napl-water flow in the vadose zone accounting for residual napl in strongly water-wet porous media. J. Contam. Hydrol. 73 (1-4), 281-304.

Oostrom, M., Rockhold, M.L., Thorne, P.D., Last, G.V., and Truex, M.J., 2003b. Three dimensional modeling of DNAPL movement and redistribution in the subsurface of the 216-Z-9 Trench at the Hanford Site. PNNL, Richland, WA.

Piepho, M.G., 1996. Numerical analysis of carbon tetrachloride movement in the saturated and unsaturated zones in the 200 West area, Hanford Site. BHI-00459, Rev. 0, Bechtel Hanford, Inc., Richland, WA.

Rohay, V.J., 1996. Field tests of passive soil vapor extraction systems at the Hanford Site, Washington. BHI-00766. Rev. 0., Bechtel Hanford, Inc., Richland, WA.

Rohay, V.J., 2000. Performance evaluation report for soil vapor extraction operations at the carbon tetrachloride site, February 1992 - September 1999. BHI-00720, Rev. 4., Richland, WA

Serne,R.J., Mitroshkov, A.V., Serne, J.N., Bjornstad, B.N., LeGore, V.L., Last, G.V., Schaef, H.T., O'Hara, M.J., Smith,S.C., Williams, B.A., Brown, C.W., Lindenmeier, C.W., Lanigan, D.C., Parker, K.E., Zachara, J.M., Horton, D.G., Kutnyakov, I.V., Burke, D.B., Clayton, R.E., 2002. Characterization of vadose zone sediment: Uncontaminated RCRA borehole core samples and composite samples. PNNL-13757. PNNL, Richland, WA.

Smith, J., C. Chiou, J. Kammer, and D. Kile. 1990. Effect of soil moisture on the sorption of trichloroethylene vapor to vadose-zone soil at Picatinny Arsenal, New Jersey. Environ. Sci. Technol. 24:676-683.

Werth, C.J. and M. Reinhard. 1997. Effects of temperature on trichloroethylene desorption from silica gel and natural sediments: 2. Kinetics. Environ. Sci. Technol. 31:697– 703.

Weitkamp, J., Ernst, S, Gunzel, B, and Deckwer, W.D., 1991. Separation of gaseous water ethanol mixtures by adsorption on hydrophobic zeolites. ZEOLITES 11 (4): 314-317.

William, B.A., Bjornstad, B.N., Schalla, R., Webber, W.D., 2002. Revised hydrogeology for the suprabasalt aquifer system, 200-West area and vicinity, Hanford Site, Washington. PNNL-13858. PNNL, Richland, WA.

Yoon, H., Valocchi, A.J., and Werth, C.W., 2003. Modeling the influence of water content on soil vapor extraction, *Vadose Zone Journal*, 2, 368-381.

Yoon, H., Valocchi, A.J., and Werth, C.W., 2004. Impact of spatially distributed nonaqueous phase liquid saturation and water content on soil vapor extraction in heterogeneous porous media, pp. 757-786, in Computational Methods in Water Resources XV, edited by C.T. Miller, M.W. Farthing, W.G. Gray, and G.F. Pinder, Elsevier.

Yoon, H., Valocchi, A.J., and Werth, C.W., 2004. Effect of soil moisture dynamics on dense nonaqueous phase liquid (DNAPL) spill zone architecture in heterogeneous porous media, *J. Contam.,Hydrol.*, submitted.